Science Advances
AAAS

Supplementary Materials for

U.S. fires became larger, more frequent, and more widespread in the 2000s

Virginia Iglesias*, Jennifer K. Balch, William R. Travis

*Corresponding author. Email: virginia.iglesias@colorado.edu

Published 16 March 2022, *Sci. Adv.* **8**, eabc0020 (2022)
DOI: 10.1126/sciadv.abc0020

This PDF file includes:

Supplementary Materials

Detection of temporal changes in fire

Time domain

We performed breakpoint analysis to estimate the optimal number and location of shifts in weekly area burned, number of fires ignited per week, and medium fire size between 1984 and 2018 in the West, Great Plains, and East. Given that these estimates are sensitive to the methodological assumptions of the analysis, we employed five frameworks to identify the optimal number of partitions: Bai and Perron's extension of the *F*-test, model selection through minimization of the Bayesian Information Criterion (BIC), regression trees, Priyadarshana et al.'s cross-entropy method, and Lavielle's penalized likelihood rupture location. Bai and Perron (*65*) extended the *F*-statistics approach, which typically tests against a single-shift alternative, to *n* against *n*+1 breaks with arbitrary but fixed *n*. Specifically, we considered the standard linear regression model [1]:

$$[1] \qquad y_t = \alpha + \beta_t^* t + \varepsilon_t \qquad (t = 1, 2, \ldots, n),$$

where y_t was either weekly area burned, number of fires ignited per week, or median fire size at time *t;* α was an intercept; β_t was a vector of linear coefficients of regression; and ε_t were the residuals of the model at time *t*;

and tested the null hypothesis that the regression coefficients β_t remained constant between 1984 and 2018 [2]:

$$[2] \qquad H_0: \beta_t = \beta_0 \qquad (t = 1, 2, \ldots, n).$$

To perform this analysis, we estimated the Optimal Least Squares (OLS) residuals from a series of segmented regression models with breakpoints *t*, …, *t* + *N*, where [3]:

$$[3] \qquad N_i = L_i * h; \qquad (L_i = \text{length of the time series}_i; \text{ and } h\text{: trimming parameter} = 0.1);$$

and compared them to the residuals from the unsegmented model via *F*-tests. We rejected the null hypothesis of no structural change when the supremum of the sequence of *F*-statistics exceeded the 0.05 *alpha*-level (*66*). Sequences of *F*-statistics show a peak with a statistically-significant maximum in 1998-1999 for weekly area burned, number of fires, and median fire size in the West, and number of fires per week in the East; as well as a peak with a statistically-significant maximum in weekly area burned and number of fires per week in the Great Plains. No statistically-significant peaks were detected for weekly area burned in the East or fire size in the Great Plains or the East (Fig. S1).

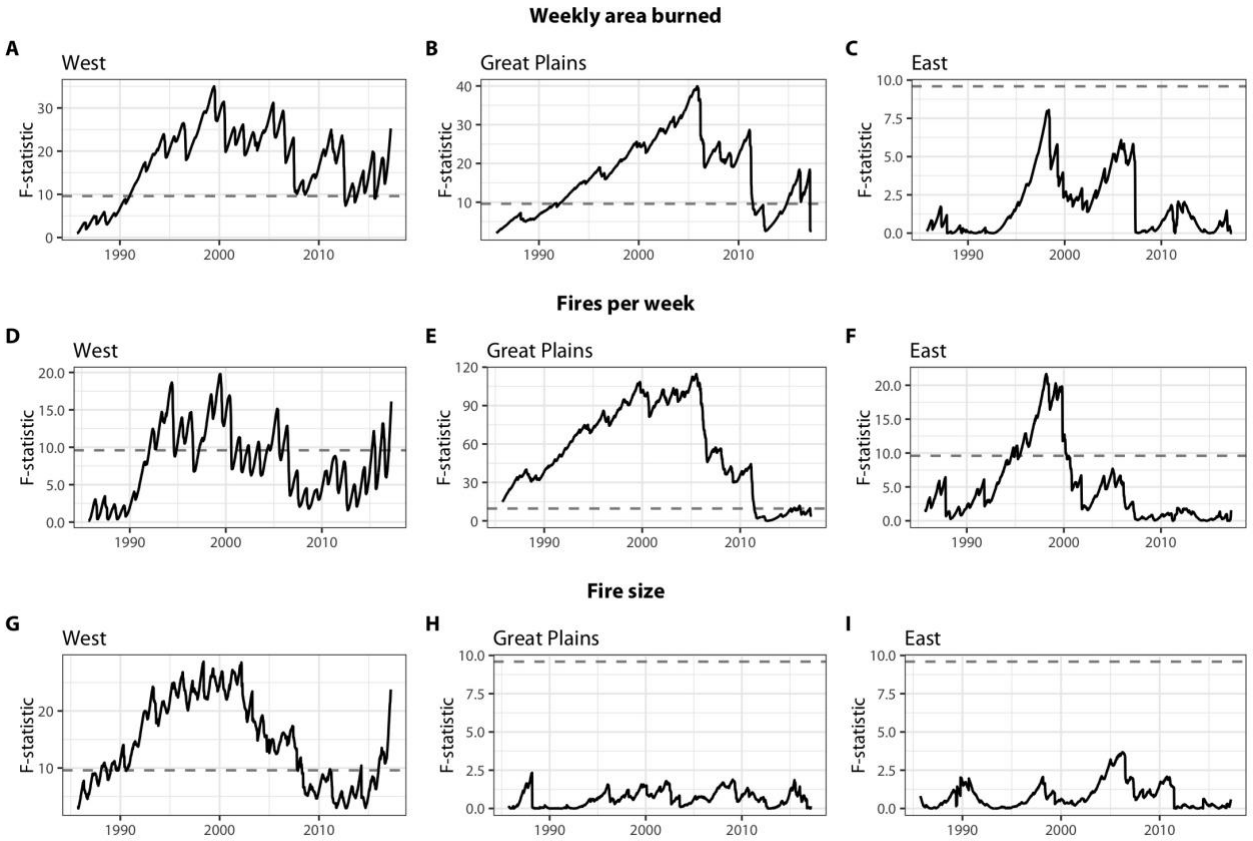

Fig. S1. Sequence of *F*-statistics for (A-C) weekly area burned, (D-F) fires ignited per week, and (G-I) median fire size between 1984 and 2018. Dashed gray lines show the 0.05 significance-level boundaries for each time series.

Following Zeileis et al. (*67*), we then fitted a series of m-segment models for $m = 0, 1, \ldots, M$, where [4]

[4] $M_i = L_i * h$; (L_i = length of the time series$_i$; and h: trimming parameter = 0.1);

and compared them based on their Residual Sum of Squares (RSS) and Bayesian Information Criterion values (BIC). The BIC is a performance score estimated as a function of penalized likelihood maximization (*68*), which has been shown to provide a reliable means to select the optimal number of breakpoints in a time series. We used Kass and Rafteri's (*69*) classification to compare BIC's (Fig. S2).

For all m's, the residual sum of squares decreases as a function of the number of breakpoints. Minimization of the BIC, nonetheless, suggests that there is very strong evidence against no changes in mean number of fires ignited per week, or mean area burned per week in the West ($(BIC_{m=0} - BICm_{m=1}) > 14$) and strong evidence against no changes in mean number of fires ignited per week in the East ($8 < (BIC_{m=0} - BIC_{m=1}) < 14$). In these three cases, BIC's monotonically increase for $m > 1$, providing strong support to the models with one breakpoint in the West (breakpoints at second week of June, 1999 for number of weekly fires; and first week of June, 2005 for area burned) and support to the model with one breakpoint fitted to the weekly number of events in the East (breakpoints at second week of May, 1998). The lowest BIC for the set of models with $m = 0, 1, \ldots, M$ fitted to weekly area burned in the East corresponds to that where $m = 0$, which suggests that there is not sufficient evidence against temporal changes in the mean (Fig. S2).

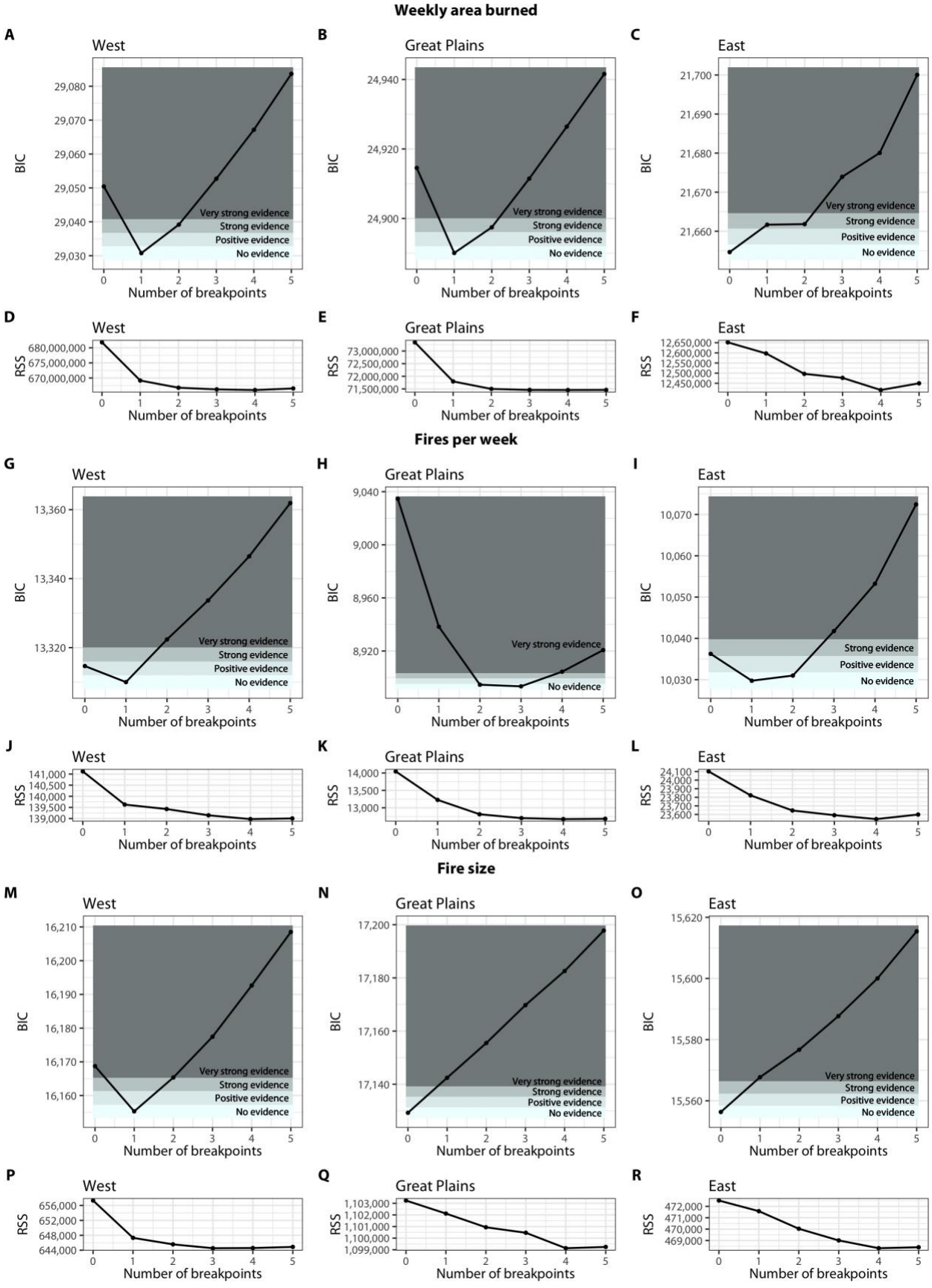

Fig. S2. Bayesian Information Criterion (BIC) and Residual Sum of Squares (RSS) for models with *m* = 0, …, 5 breakpoints and fitted to (A-F) weekly area burned, (G-L) number of fires ignited per week, and (M-

R) median fire size in the West, Great Plains, and East. The shading represents the strength of the evidence against models with BIC's higher than the minimum BIC computed for each set of models.

Third, we applied regression trees to split the time series of weekly area burned, number of fires ignited per week, and median fire size in the West, Great Plains, and East. The algorithm is free of distributional assumptions, and grows the tree by performing binary recursive partitioning. At each step, nodes are defined at points where the partitioning of the dataset leads to the lowest Gini impurity (*70*). The Gini impurity is a metric used in information theory to assess the likelihood of incorrect classification. Given that this top-down method of partitioning is known to overestimate the number of breakpoints (*71*), we cross-validated the preliminary trees and pruned the results to estimate the optimal number of partitions.

The best classification, as inferred from maximization of the reduction of the Gini impurity, was obtained for trees with five terminal nodes for weekly area burned in the West; three terminal nodes for number of fires ignited per week and median fire size in the West, as well as for weekly area burned in the Great Plains; ten terminal nodes for fires ignited per week in the Great Plains; and two terminal nodes for fires ignited per week in the East. Cross-validation of the trees indicates that these numbers of nodes are associated with the largest reduction of the deviance, with the exception of the model fit to fires ignited per week in the Great Plains, where deviance is minimized in a tree with six nodes (Fig. S3). Regression trees thus suggest that optimal partitioning is achieved with breakpoints (breakpoints = nodes - 1) corresponding to years 1999 and 2005- 2006 for weekly area burned in the West and Great Plains, respectively; 2018 (West), 2005, 2006, 2011, and 2012 (Great Plains), and 1998 (East) for fires ignited per week; and 1998 for median fire size in the West. Single-node trees for median fire size in the Great Plains and East as well as weekly area burned in the East indicate that sequential partitioning of these time series did not identify statistically significant breakpoints.

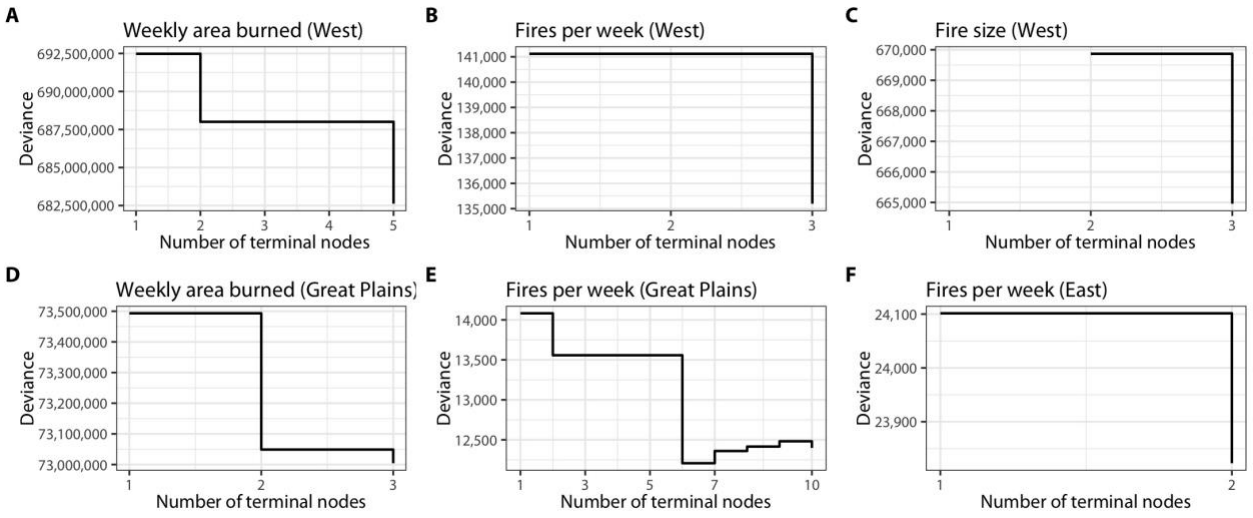

Fig. S3. Changes in deviance for trees with more than two terminal nodes. The largest *n*'s shown in the figure correspond to the number of terminal nodes identified by the regression trees prior to pruning.

Fourth, we employed Priyadarshana et al.'s cross-entropy method for detection of multiple breakpoints associated with structural changes in a series (*72*). The algorithm is designed to test the hypothesis that an unknown number of breakpoints divide the time series in segments generated by a distribution inherent to the underlying process. We assumed the distribution to be normal for area burned per week and fire size, and negative binomial for number of fires

ignited per week. A truncated normal distribution was then used to simulate *m* breakpoints, where $m = 0, 1, \ldots, M$ [4]. The segmentation that minimized the Bayesian Information Criterion was considered the optimal solution. The analysis suggests that changes in weekly area burned occurred in 2001, 2002, and 2005 in the West; in 2001 and 2002 in the Great Plains; and 1998 and 1999 in the East. Shifts in number of fires ignited per week were registered in 2001 and 2002 in the West; 1986 and 1999 in the Great Plains; and 1999, 2002, and 2004 in the East. Changes in fire size were detected in 2002 in the West, and in 2002 and 2003 in the Great Plains.

Finally, we applied a dynamic programing approach to find the optimal segmentation with 1 to 50 breakpoints in each time series (*73, 74*). We then estimated the number of breakpoints by minimizing the penalized contrast function ((*75*); Fig S4). Time series segmentation indicates the presence of breakpoints in weekly area burned (in 1996 and 1999 in the West, in 2005 in the Great Plains, and in 1998 and 1999 in the East), number of fires ignited per week (in 1989 and 1994 in the West and 1998 in the Great Plains); and median fire size (1998 in the West and 1988 in the Great Plains).

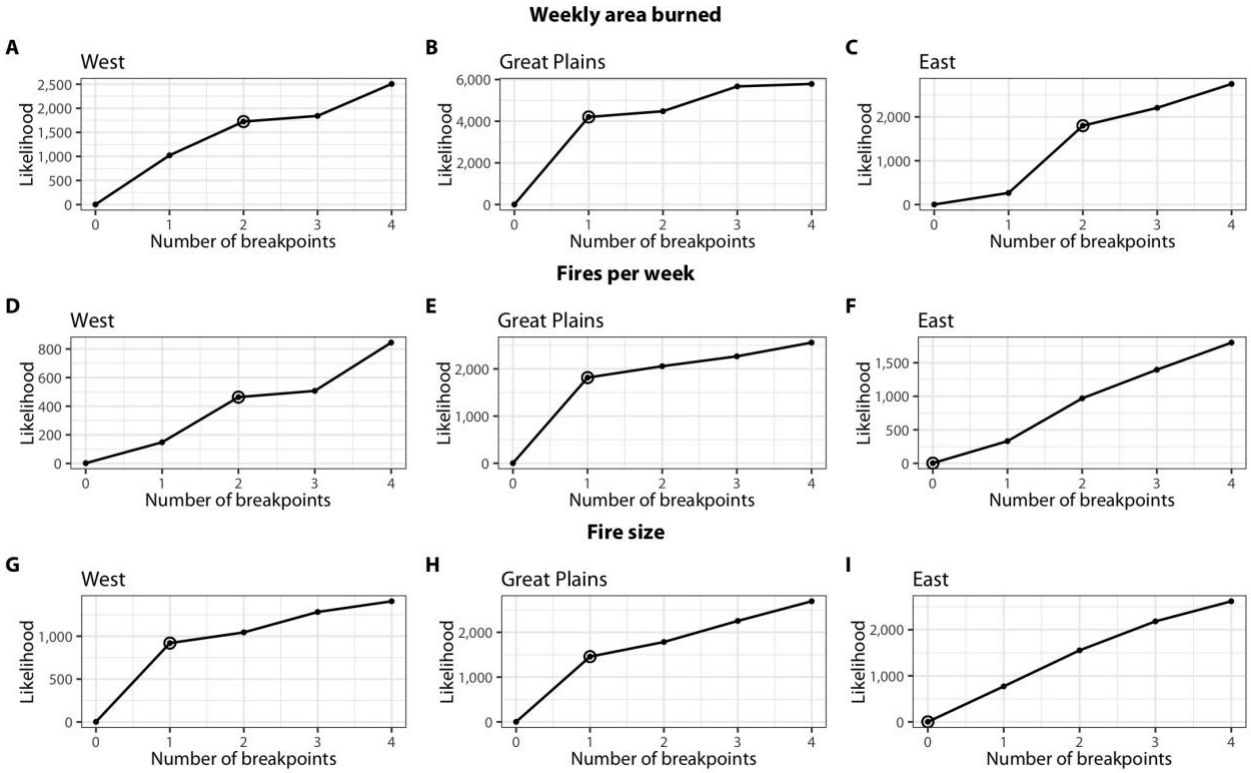

Fig. S4. Likelihood of the optimal segmentation estimated through dynamic programming for 1 to 5 breakpoints. The circles show the number of breakpoints that minimize the penalized contrast function.

Despite different parametrization, penalization criteria and distribution assumptions, all five tests identified structural changes in the time series of weekly area burned in the West and Great Plains, and median fire size in the West in 1998-2002, while three tests point to shifts in weekly area burned in the East and fires ignited per week in the West over the same period. Two breakpoints are inferred for fires ignited per week in the Great Plains, the first one in 1999 and the most recent one in 2005. These breakpoints are supported by three and four tests, respectively. Breakpoints for area burned per week in the West were detected in 2005. No changes in median fire size in the Great Plains or East were detected by more than one test (Fig. S5).

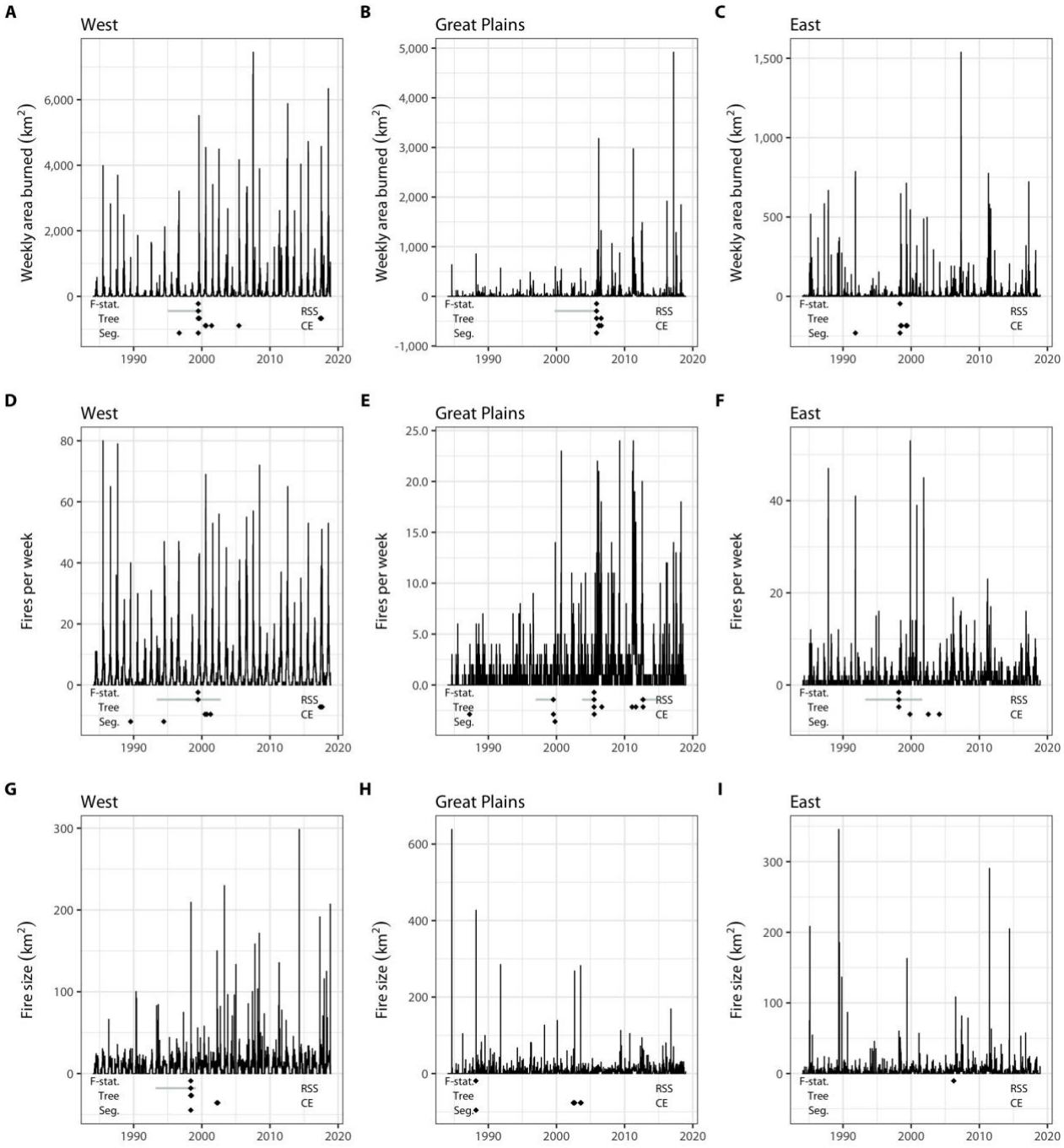

Fig S5. Temporal trends in weekly area burned (A-C), number of fires ignited per week (D-F), and median fire size (G-H). Breakpoints identified by extension of the *F*-test ('F-stat.'), segmentation through Residual Sum of Squares ('RSS') and Bayesian Information Criterion optimization, regression trees ('Tree'), a cross-entropy method ('CE'), and a programming approach to segmentation ('Seg.').

Frequency domain

We computed the power spectrum of area burned in the West, Great Plains and East by applying the continuous Morlet wavelet transform at a daily resolution ((*47*); Fig. 1 J-L). Following Scafetta et al. (*10*), we then calculated the wavelet transform modulus maxima line tree (WTMM) of each series to detect the location of irregular structures and linked them to their position in time (Fig. S1 A-C). Given that the spectrum of singularities may present problems of stability, we fitted linear models to the log-log transformed WTMM space versus

a coefficient that measures the width of a wavelet known as scale (s) on the scale interval $1 \leq s \leq 10$ (*76*). The resulting scaling exponent is an approximation to the local Hölder exponent h at each singularity ((*77*); 1992; Fig S6 D-F). Finally, we divided the time series from each region in two periods, i.e., 1984–1999 and 2005–2018, and estimated the probability of changes in Hölder exponents under the null hypothesis that the mean and standard deviation of the distributions were equal in both periods (Fig. S6. G-I). The distribution of the null hypothesis was generated by randomly shuffling exponents (5000 permutations) and calculating the difference in the simulated means and standard deviations for 1984-1999 and 2005-2018.

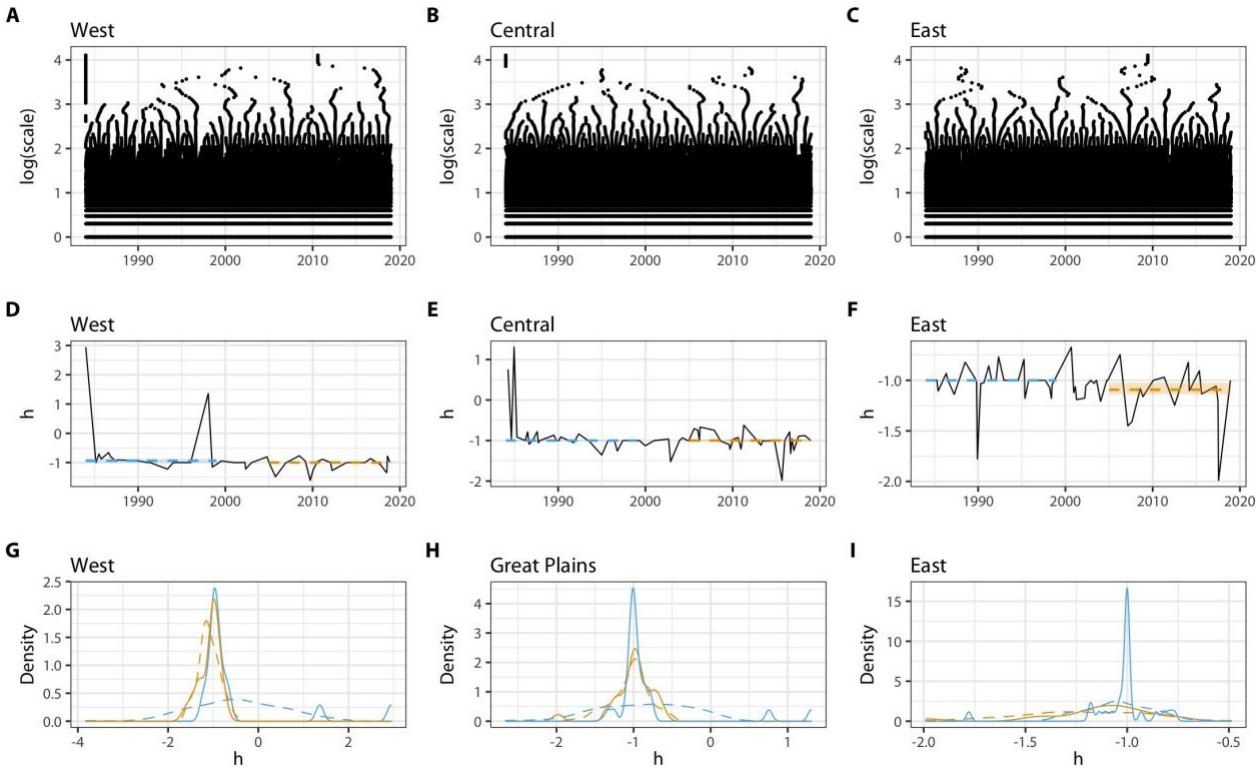

Fig S6. Hölder exponent analysis of daily area burned in the West, Great Plains and East. (A-C) **Wavelet modulus maxima for the time series** (D-F) Time series of Hörst exponents. Horizontal dashed lines show the mean Hölder exponent in 1984-1999 (in blue) and 2005-2018 (in orange). 95% confidence intervals for the estimates are represented as solid horizontal bars. (G-I) Density distribution of Hölder exponents in 1984-1999 (in blue) and 2005-2018 (in orange). For reference, a normal distribution fitted to these exponents is depicted with dashed lines.

While mean Hölder exponents ($\overline{h}$) in 1984-1998 and 2005-2018 were not statistically different in any of the regions ($p>0.05$), the standard deviations of the distributions changed ($p<0.05$). In the West and Great Plains, $-1.00 < \overline{h} < -0.50$ suggest that daily area burned behaves like stationary antipersistent noise. In the East, $\overline{h}$ of -1.03 ± 0.03 and -1.14 ± 0.07 in 1984-1998 and 2005-2018, respectively, are indicative of antipersitent but potentially nonstationary dynamics (*9*).

Comparison of Monitoring Trends in Burn Severity (MTBS), Integrated Reporting of Wildland-Fire Information (IRWIN), and Landsat Burned Area (LBA)

This study is based on data obtained from Monitoring Trends in Burn Severity (MTBS). Fire perimeter delineation is guided by state and federal fire history records and performed manually through standardized analysis of Landsat imagery (*8*). The main potential sources of error in this product are therefore associated with fire reporting errors and changes in Landsat sensors/imagery availability. Should they be temporally biased, errors in MTBS could significantly influence our results. For this reason, we compared annual time series generated from MTBS with Integrated Reporting of Wildland-Fire Information (IRWIN (*11*)), Landsat Burned Area (LBA (*12*)), and Fire Events Delineation (FIRED (*13*)).

IRWIN is a centralized interagency hub that integrates fire incidents from multiple sources. MTBS underestimates area burned in the West and overestimates area burned in the Great Plains and East with respect to IRWIN. Although the variability was larger prior to ~2000, we found no statistical differences in annual area burned before and after the shift (Fig. S7). Improvements in fire detection capabilities arising from better quality and/or more satellite imagery could be expected to be associated with Landsat 7 and its Enhanced Thematic Mapper Plus sensor (ETM+). Those improvements would have resulted in an overestimation of area burned by MTBS with respect to IRWIN after 1999. No changes in the MTBS-to-IRWIN area burned ratio argues against a temporal bias in the fire time series introduced by the availability of imagery from Landsat 7.

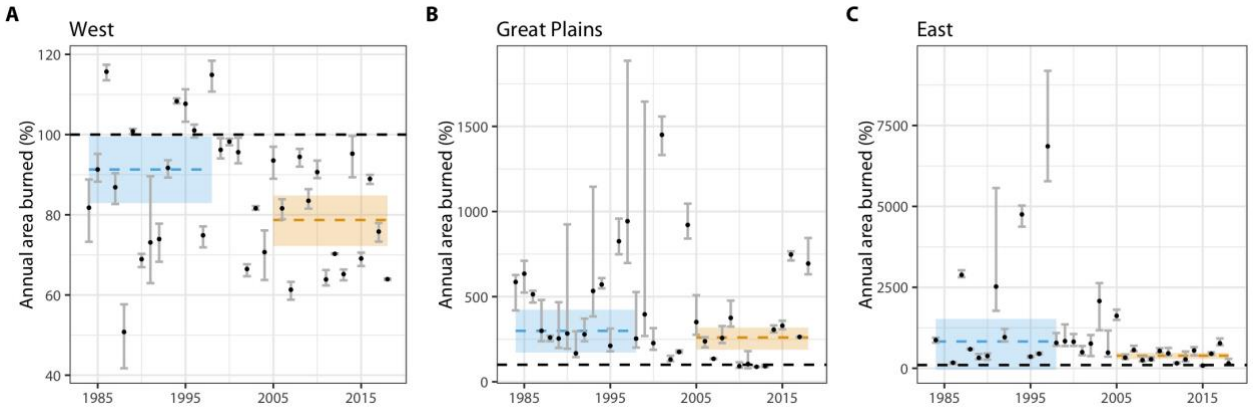

Fig. S7. MTBS-to-IRWIN derived annual area burned for the (A) West, (B) Great Plains, and (C) East. Dots represent mean values and whiskers, the standard deviation. Mean ratios for 1984-1998 and 2005-2018 are depicted in blue and orange, respectively.

Imagery from both Landsat 5 Thematic Mapper and Landsat 7 ETM+ is available for 1999-2013. Comparison of area burned derived with the Landsat Burn Area algorithm (LBA) from imagery obtained from both sensors suggests that there are no differences between products (Fig. S8; (*12*)). LBA is an algorithm that uses machine learning, thresholding and image segmentation to derive time series of area burned from Landsat imagery (*12*).

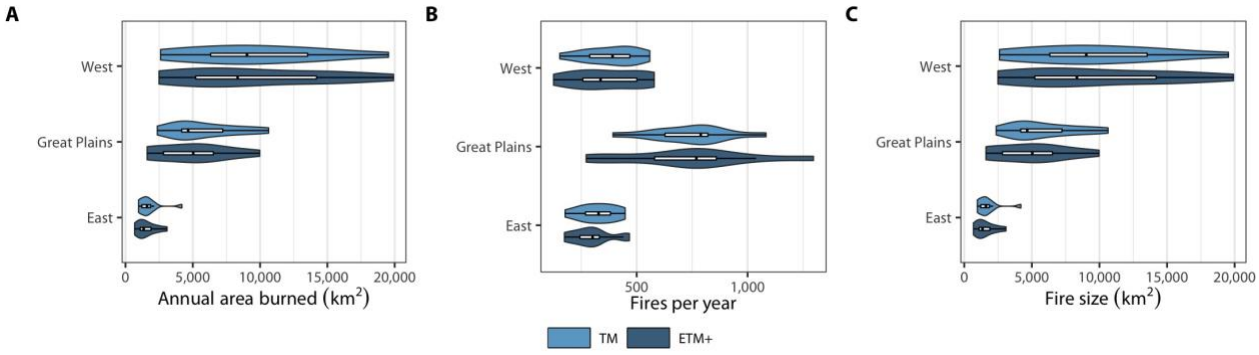

Fig. S8. Comparison of fire products derived from TM and ETM+ with the Landsat Burn Area algorithm for the West, Great Plains and East. (A) Annual area burned. (B) Fires per year. (C) Median fire size.

As expected, time series of annual area burned, fires per year, and fire size derived from TM and ETM+ scenes are notably similar. Further, they show no indication of temporal biases when compared against Fire Events Delineation (FIRED), an algorithm derived from the MODIS Burned Area Product (Fig. S9).

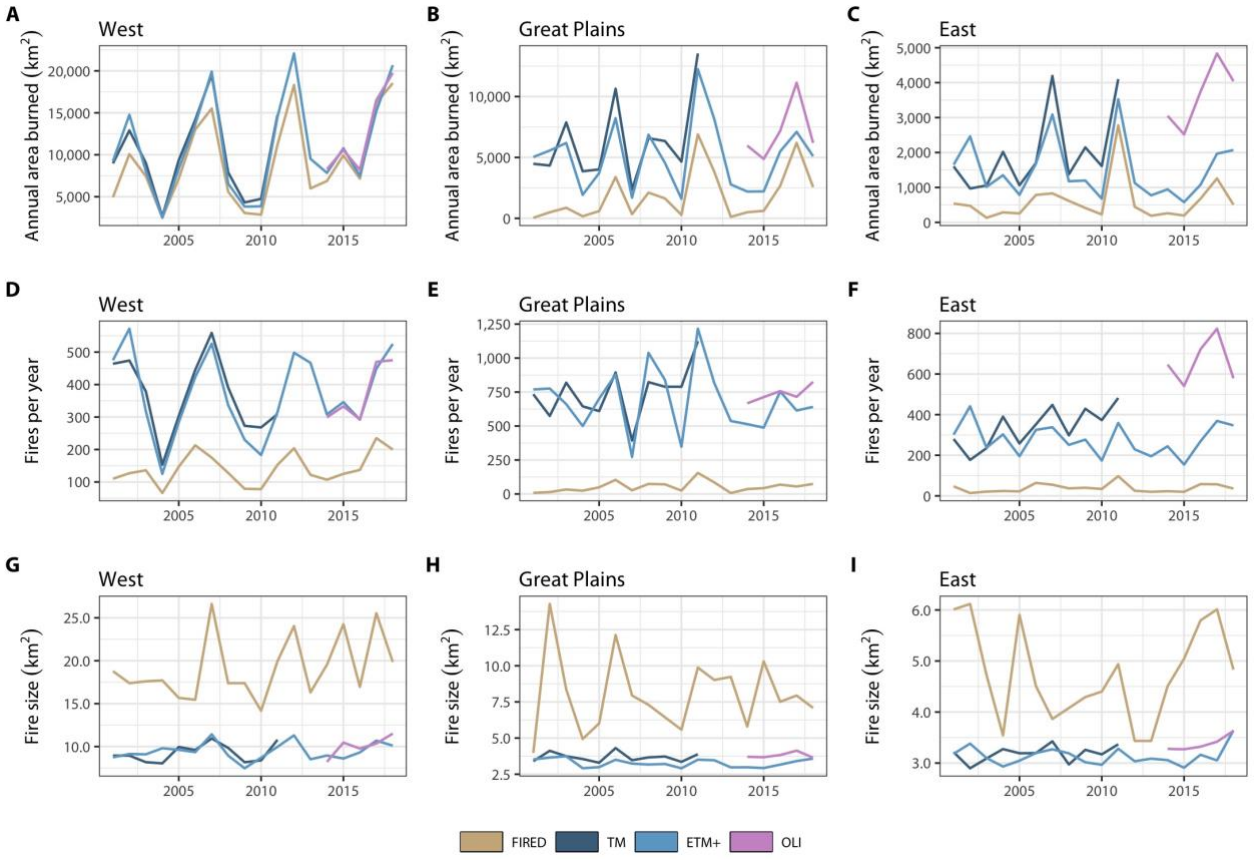

Fig. S9. Time series derived from MODIS (Fire Events Delineation algorithm; FIRED) and Landsat's Thematic Mapper (TM), Enhanced Thematic Mapper Plus (ETM+), and Operational Land Imager (OLI) sensors. (A-C) Annual area burned. (D-F) Number of fires ignited per year. (G-I) Median fire size.

Table S1. Annual area burned in 1984-1998 and 2005-2018 as estimated from MTBS. Asterisks indicate that the differences between periods are statistically different (*pseudo*-p<0.05).

Region	Mean (km^2)		Median (km^2)		99th quantile (km^2)	
	1984 - 1998	**2005 - 2018**	**1984 - 1998**	**2005 - 2018**	**1984 - 1998**	**2005 - 2018**
West	5330.63 ± 988.88	14,890.63 ± 1834.36*	4019.26 ±1203.59	14,249.40 ± 3097.77*	9837.33 ± 2767.26	24,102.00 ± 1941.66*
Great plains	826.41 ± 189.17	3947.07 ± 921.20*	542.41 ± 214.63	3354.09 ± 1314.34*	2253.02 ± 686.59	9317.08 ± 2072.28*
East	887.02 ± 202.92	1434.41 ± 360.88	537.78 ± 356.34	833.34 ± 218.73	2143.43 + 298.19	4581.79 ± 1492.23*

Table S2. Number of fires per year in 1984-1998 and 2005-2018 as estimated from MTBS. Asterisks indicate that the differences between periods are statistically different (*pseudo*-p<0.05).

Region	Mean		Median		99th quantile	
	1984 - 1998	**2005 - 2018**	**1984 - 1998**	**2005 - 2018**	**1984 - 1998**	**2005 - 2018**
West	174 ± 21	270 ± 21*	156 ± 27	266 ± 31*	328 ± 44*	400 ± 37*
Great plains	34 ± 5	113 ± 20*	27 ± 5	104 ± 14*	63 ± 11*	230 ± 73*
East	57 ± 8	94 ± 13*	53 ± 10	78 ± 16	101 ± 18	148 ± 37

Table S3. Fire size in 1984-1998 and 2005-2018 as estimated from MTBS. Asterisks indicate that the differences between periods are statistically different (*pseudo*-p<0.05).

Region	Mean (km^2)		Median (km^2)		99th quantile (km^2)	
	1984 - 1998	**2005 - 2018**	**1984 - 1998**	**2005 - 2018**	**1984 - 1998**	**2005 - 2018**
West	30.62 ± 1.54	55.21 ± 2.37*	12.11 ± 0.27	15.09 + 0.48*	284.76 ± 34.79	693.67 ± 64.12*
Great plains	24.55 ± 2.80	34.89 ± 3.10*	9.84 ± 0.50	10.34 ± 0.24	222.67 ± 87.35	426.92 ± 83.08*
East	15.65 ± 1.45	15.31 ± 1.60	5.06 ± 0.19	4.99 ± 0.14	208.43 ± 56.03	156.47 ± 28.99

Table S4. Annual area burned in 1984-1998 and 2005-2018 as estimated from IRWIN. Asterisks indicate that the differences between periods are statistically different (*pseudo*-p<0.05).

Region	Mean (km^2)		Median (km^2)		99th quantile (km^2)	
	1984 - 1998	**2005 - 2018**	**1984 - 1998**	**2005 - 2018**	**1984 - 1998**	**2005 - 2018**
West	6188.76 ± 1195.54	20,352.47 ± 3057.14*	4429.5 ± 1379.49	18,500.74 ± 5072.47*	14,993.26 ± 3495.18	37,369.1 ± 3953.23*
Great plains	240.27 ± 63.16	2212.41 ± 809.44*	166.67 ± 60.35	666.94 ± 67.92*	682.53 ± 226.61	6776.52 ± 3040.96*
East	135.63 ± 47.58	380.46 ± 77.01*	82.11 ± 31.14	315.69 ± 77.01*	336.37 ± 209.37	811.61 ± 220.66*

Table S5. Number of fires per year in 1984-1998 and 2005-2018 as estimated from IRWIN. Asterisks indicate that the differences between periods are statistically different (*pseudo*-p<0.05).

Region	Mean		Median		99th quantile	
	1984 - 1998	**2005 - 2018**	**1984 - 1998**	**2005 - 2018**	**1984 - 1998**	**2005 - 2018**
West	188 ± 22	307 ± 28*	165 ± 31	274 ± 43*	293 ± 37	460 ± 34*
Great plains	8 ± 2	41 ± 9*	7 ± 1	30 ± 8*	13 ± 9	70 ± 34*
East	10 ± 2	21 ± 2*	10 ± 3	20 ± 5*	19 ± 2	32 ± 3*

Table S6. Fire size in 1984-1998 and 2005-2018 as estimated from IRWIN. Asterisks indicate that the differences between periods are statistically different (*pseudo*-p<0.05).

Region	Mean (km^2)		Median (km^2)		99th quantile (km^2)	
	1984 - 1998	**2005 - 2018**	**1984 - 1998**	**2005 - 2018**	**1984 - 1998**	**2005 - 2018**
West	32.94 ± 1.55	66.34 ± 2.75*	11.85 ± 0.29	16.8 ± 0.45*	341.03 ± 65.13	902.41 ± 66.29*
Great plains	28.83 ± 5.52	53.68 ± 9.18*	9.13 ± 1.87	8.21 ± 0.57	212.71 ± 104.18	757.99 ± 238.46*
East	13.56 ± 3.04	18.12 ± 2.84	4.46 ± 0.37	4.69 ± 0.33	148.68 ± 72.74	275.3 ± 92.02

Table S7. Annual area burned in 1984-1998 and 2005-2018 as estimated from LBA. Asterisks indicate that the differences between periods are statistically different (*pseudo*-p<0.05).

Region	Mean (km^2)		Median (km^2)		99th quantile (km^2)	
	1984 - 1998	**2005 - 2018**	**1984 - 1998**	**2005 - 2018**	**1984 - 1998**	**2005 - 2018**
West	5474.84 ± 791.7	12,026.06 ± 1510.24*	4234.77 ± 882.12	10,147.13 ± 2348.73*	9899.69 ± 2093.43	20,681.67 ± 2352.1*
Great plains	4201.98 ± 549.76	5797.68 ± 881.98*	3473.2 ± 722.51	5298.52 ± 951.35*	7848.08 ± 1288.47	10,636.98 ± 2392.04
East	1312.34 ± 158.72	1766.15 ± 285.66*	1081.62 ± 253.07	1493.94 ± 287.37	2341.64 ± 289.78	4101.05 ± 1002.42*

Table S8. Number of fires per year in 1984-1998 and 2005-2018 as estimated from LBA. Asterisks indicate that the differences between periods are statistically different (*pseudo*-p<0.05).

Region	Mean		Median		99th quantile	
	1984 - 1998	**2005 - 2018**	**1984 - 1998**	**2005 - 2018**	**1984 - 1998**	**2005 - 2018**
West	301 ± 27	388 ± 26*	295 ± 52	368 ± 52	460 ± 22	525 ± 34*
Great plains	577 ± 54	699 ± 49*	558 ± 53	698 ± 78*	970 ± 162	894 ± 122
East	259 ± 28	318 ± 26*	227 ± 44	322 ± 40*	419 ± 72	448 ± 35

Table S9. Fire size in 1984-1998 and 2005-2018 as estimated from LBA. Asterisks indicate that the differences between periods are statistically different (*pseudo*-p<0.05).

Region	Mean (km^2)		Median (km^2)		99th quantile (km^2)	
	1984 - 1998	**2005 - 2018**	**1984 - 1998**	**2005 - 2018**	**1984 - 1998**	**2005 - 2018**
West	18.22 ± 0.67	30.99 ± 1.27*	8.3 ± 0.11	9.6 ± 0.15*	148.92 ± 7.15	388.50 ± 38.72*
Great plains	7.28 ± 0.22	8.30 ± 0.31*	3.44 ± 0.03	3.45 ± 0.03	60.70 ± 4.39	81.44 ± 5.58*
East	5.06 ± 0.19	5.56 ± 0.32	3.13 ± 0.04	3.2 ± 0.03	30.47 ± 2.2	35.63 ± 3.49

REFERENCES AND NOTES

1. A. C. Scott, I. J. Glasspool, The diversification of Paleozoic fire systems and fluctuations in atmospheric oxygen concentration. *Proc. Natl. Acad. Sci. U.S.A.* **103**, 10861–10865 (2006).

2. J. Williams, L. Hamilton, R. Mann, M. Rousanville, H. Leonard, O. Daniels, D. Bunnell, S. Mann, *The Mega-Fire Phenomenon: Toward a More Effective Management Model* (The Brookings Institution, Center for Public Policy Education, 2005).

3. S. J. Pyne, in *Proceedings of the 4th International Wildland Fire Conference*, Seville, Spain, 13 to 17 May 2007 (2007), pp. 1–7.

4. P. Attiwill, D. Binkley, Exploring the mega-fire reality: A 'forest ecology and management' conference. *For. Ecol. Manage.* **294**, 1–3 (2013).

5. CEMHS, *Spatial Hazard Events and Losses Database for the United States* (Center for Emergency Management and Homeland Security, Arizona State University, 2019); https://sheldus.asu.edu/SHELDUS/.

6. P. E. Dennison, S. C. Brewer, J. D. Arnold, M. A. Moritz, Large wildfire trends in the western United States, 1984-2011. *Geophys. Res. Lett.* **41**, 2928–2933 (2014).

7. L. Shore, "2016–2018 southern plains wildfire assessment" (Oklahoma Panhandle Research and Extension Center, 2019), p. 26.

8. J. Eidenshink, B. Schwind, K. Brewer, Z.-L. Zhu, B. Quayle, S. Howard, A project for monitoring trends in burn severity. *Fire Ecol.* **3**, 3–21 (2007).

9. B. Mandelbrot, *The Fractal Geometry of Nature* (Freeman, 1983).

10. N. Scafetta, L. Griffin, B. J. West, Hölder exponent spectra for human gait. *Phys. A Stat. Mech. Appl.* **328**, 561–583 (2003).

11. IRWIN, *Integrated Reporting of Wildland-Fire Information (IRWIN)*; www.forestsandrangelands.gov/WFIT/applications/IRWIN/index.shtml.

12. T. J. Hawbaker, M. K. Vanderhoof, G. L. Schmidt, Y.-J. Beal, J. J. Picotte, J. D. Takacs, J. T. Falgout, J. L. Dwyer, The Landsat Burned Area algorithm and products for the conterminous United States. *Remote Sens. Environ.* **244**, 111801 (2020).

13. J. K. Balch, L. A. St. Denis, A. L. Mahood, N. P. Mietkiewicz, T. M. Williams, J. McGlinchy, M. C. Cook, FIRED (Fire Events Delineation): An open, flexible algorithm and database of US fire events derived from the MODIS Burned Area Product (2001–2019). *Remote Sens. (Basel)* **12**, 3498 (2020).

14. M. B. Joseph, M. W. Rossi, N. P. Mietkiewicz, A. L. Mahood, M. E. Cattau, L. A. St. Denis, R. C. Nagy, V. Iglesias, J. T. Abatzoglou, J. K. Balch, Spatiotemporal prediction of wildfire size extremes with Bayesian finite sample maxima. *Ecol. Appl.* **29**, e01898 (2019).

15. A. L. Westerling, M. G. Turner, E. A. H. Smithwick, W. H. Romme, M. G. Ryan, Continued warming could transform Greater Yellowstone fire regimes by mid-21st century. *Proc. Natl. Acad. Sci. U.S.A.* **108**, 13165–13170 (2011).

16. F. Tedim, V. Leone, M. Amraoui, C. Bouillon, M. Coughlan, G. Delogu, P. Fernandes, C. Ferreira, S. McCaffrey, T. McGee, J. Parente, D. Paton, M. Pereira, L. Ribeiro, D. Viegas, G. Xanthopoulos, Defining extreme wildfire events: Difficulties, challenges, and impacts. *Fire* **1**, 9 (2018).

17. J. K. Balch, V. Iglesias, A. Braswell, M. W. Rossi, M. B. Joseph, A. L. Mahood, T. Shrum, C. White, V. Scholl, B. McGuire, C. Karban, M. Buckland, W. Travis, Social-environmental extremes: Rethinking extraordinary events as outcomes of interacting biophysical and social systems. *Earth's Future* **8**, e2019EF001319 (2020).

18. B. D. Malamud, G. Morein, D. L. Turcotte, Forest fires: An example of self-organized critical behavior. *Science* **281**, 1840–1842 (1998).

19. D. V. Spracklen, L. Garcia-Carreras, The impact of Amazonian deforestation on Amazon basin rainfall. *Geophys. Res. Lett.* **42**, 9546–9552 (2015).

20. X. Yue, L. J. Mickley, J. A. Logan, Projection of wildfire activity in southern California in the mid-twenty-first century. *Climate Dynam.* **43**, 1973–1991 (2014).

21. J. C. Liu, L. J. Mickley, M. P. Sulprizio, F. Dominici, X. Yue, K. Ebisu, G. B. Anderson, R. F. A. Khan, M. A. Bravo, M. L. Bell, Particulate air pollution from wildfires in the Western US under climate change. *Clim. Change* **138**, 655–666 (2016).

22. M. I. Bogachev, J. F. Eichner, A. Bunde, Effect of nonlinear correlations on the statistics of return intervals in multifractal data sets. *Phys. Rev. Lett.* **99**, 240601 (2007).

23. D. McKenzie, M. C. Kennedy, Power laws reveal phase transitions in landscape controls of fire regimes. *Nat. Commun.* **3**, 726 (2012).

24. Texas A&M Forest Service, "2011 Texas wildfires: Common denominators of home destruction" (A&M Forest Service, 2011), p. 50.

25. A. S. Sharma, D. N. Baker, A. Bhattacharyya, A. Bunde, V. P. Dimri, H. K. Gupta, V. K. Gupta, S. Lovejoy, I. G. Main, D. Schertzer, H. von Storch, N. W. Watkins, in *Geophysical Monograph Series*, A. S. Sharma, A. Bunde, V. P. Dimri, D. N. Baker, Eds. (American Geophysical Union, 2012), vol. 196, pp. 1–16; https://agupubs.onlinelibrary.wiley.com/doi/10.1029/2012GM001233.

26. J. T. Abatzoglou, C. A. Kolden, Relationships between climate and macroscale area burned in the western United States. *Int. J. Wildland Fire* **22**, 1003 (2013).

27. J. S. Littell, D. McKenzie, D. L. Peterson, A. L. Westerling, Climate and wildfire area burned in western U.S. ecoprovinces, 1916–2003. *Ecol. Appl.* **19**, 1003–1021 (2009).

28. R. Seager, D. Neelin, I. Simpson, H. Liu, N. Henderson, T. Shaw, Y. Kushnir, M. Ting, B. Cook, Dynamical and thermodynamical causes of large-scale changes in the hydrological cycle over North America in response to global warming. *J. Climate* **27**, 7921–7948 (2014).

29. J. T. Abatzoglou, A. P. Williams, Impact of anthropogenic climate change on wildfire across western US forests. *Proc. Natl. Acad. Sci. U.S.A.* **113**, 11770–11775 (2016).

30. A. P. Williams, E. R. Cook, J. E. Smerdon, B. I. Cook, J. T. Abatzoglou, K. Bolles, S. H. Baek, A. M. Badger, B. Livneh, Large contribution from anthropogenic warming to an emerging North American megadrought. *Science* **368**, 314–318 (2020).

31. Y. Zhuang, R. Fu, B. D. Santer, R. E. Dickinson, A. Hall, Quantifying contributions of natural variability and anthropogenic forcings on increased fire weather risk over the western United States. *Proc. Natl. Acad. Sci. U.S.A.* **118**, e2111875118 (2021).

32. J. K. Balch, B. A. Bradley, J. T. Abatzoglou, R. C. Nagy, E. J. Fusco, A. L. Mahood, Human-started wildfires expand the fire niche across the United States. *Proc. Natl. Acad. Sci. U.S.A.* **114**, 2946–2951 (2017).

33. R. C. Nagy, E. Fusco, B. Bradley, J. T. Abatzoglou, J. K. Balch, Human-related ignitions increase the number of large wildfires across U.S. ecoregions. *Fire* **1**, 4 (2018).

34. S. A. Parks, J. T. Abatzoglou, Warmer and drier fire seasons contribute to increases in area burned at high severity in western US forests from 1985 to 2017. *Geophys. Res. Lett.* **47**, e2020GL089858 (2020).

35. M. G. Turner, K. H. Braziunas, W. D. Hansen, B. J. Harvey, Short-interval severe fire erodes the resilience of subalpine lodgepole pine forests. *Proc. Natl. Acad. Sci. U.S.A.* **116**, 11319–11328 (2019).

36. E. J. Fusco, J. T. Finn, J. K. Balch, R. C. Nagy, B. A. Bradley, Invasive grasses increase fire occurrence and frequency across US ecoregions. *Proc. Natl. Acad. Sci. U.S.A.* **116**, 23594–23599 (2019).

37. J. Williams, A. Hyde, in *Society of American Foresters* (Orlando, Fl, 2009).

38. H. Stanke, A. O. Finley, G. M. Domke, A. S. Weed, D. W. MacFarlane, Over half of western United States' most abundant tree species in decline. *Nat. Commun.* **12**, 451 (2021).

39. K. E. Gleason, J. R. McConnell, M. M. Arienzo, N. Chellman, W. M. Calvin, Four-fold increase in solar forcing on snow in western U.S. burned forests since 1999. *Nat. Commun.* **10**, 2026 (2019).

40. H. Botts, S. McCabe, B. Stueck, L. Suhr, "Wildfire hazard risk" (Corelogic, 2015).

41. V. Iglesias, A. Brasswell, M. Joseph, C. McShane, M. Rossi, M. Cattau, M. Koontz, J. McGlinchy, R. Nagy, J. Balch, W. Travis, Risky development: Increasing exposure to natural hazards in the United States. *Earth's Future* **9**, e2020EF001795 (2021).

42. T. Schoennagel, J. K. Balch, H. Brenkert-Smith, P. E. Dennison, B. J. Harvey, M. A. Krawchuk, N. Mietkiewicz, P. Morgan, M. A. Moritz, R. Rasker, M. G. Turner, C. Whitlock, Adapt to more wildfire in western North American forests as climate changes. *Proc. Natl. Acad. Sci. U.S.A.* **114**, 4582–4590 (2017).

43. R. Gorte, "The rising cost of wildfire protection" (Headwaters Economics, 2013), p. 16.

44. I. P. Davies, R. D. Haugo, J. C. Robertson, P. S. Levin, The unequal vulnerability of communities of color to wildfire. *PLOS ONE* **13**, e0205825 (2018).

45. S. J. Pyne, From pleistocene to pyrocene: Fire replaces ice. *Earth's Future* **8**, e2020EF001722 (2020).

46. Commission for Environmental Cooperation, *Ecological Regions of North America: Toward a Common Perspective* (2006).

47. C. Torrence, G. P. Compo, A practical guide to wavelet analysis. *Bull. Am. Meteorol. Soc.* **79**, 61–78 (1998).

48. R Core Team, *R: A Language and Environment for Statistical Computing* (The R Foundation, 2019); www.R-project.org/.

49. A. Canty, B. Ripley, *boot: Bootstrap R (S-Plus) Functions* (2019).

50. W. Priyadarshana, G. Sofronov, *Breakpoint: An R Package for Multiple Break-Point Detection via the Cross-Entropy Method* (2019); https://CRAN.R-project.org/package=breakpoint.

51. R. Killick, I. A. Eckley, changepoint: An R package for changepoint analysis. *J. Stat. Softw.* **58**, 1–19 (2014).

52. C. Wilke, *ggridges: Ridgeline plots in "ggplot2"* (2020).

53. R. Bivand, N. Lewin-Koh, *maptools: Tools for Handling Spatial Objects* (2020); https://CRAN.R-project.org/package=maptools.

54. R. Hijmans, *raster: Geographic Data Analysis and Modeling* (2022); https://CRAN.R-project.org/package=raster.

55. R. Bivand, T. Keith, B. Rowlingson, *rgdal: Bindings for the "Geospatial" Data Abstraction Library* (2020); https://CRAN.R-project.org/package=rgdal.

56. R. Bivand, C. Rundel, *rgeos: Interface to Geometry Engine - Open Source ('GEOS')* (2020); https://CRAN.R-project.org/package=rgeos.

57. R. Bivand, E. Pebesma, V. Gomez-Rubio, *Applied Spatial Data Analysis with R* (Springer, 2013); https://asdar-book.org/.

58. A. Baddeley, E. Rubak, R. Turner, *Spatial Point Patterns: Methodology and Applications with R* (Chapman and Hall/CRC Press, 2015).

59. H. Wickham, M. Averick, J. Bryan, W. Chang, L. D. McGowan, R. François, G. Grolemund, A. Hayes, L. Henry, J. Hester, M. Kuhn, T. L. Pedersen, E. Miller, S. M. Bache, K. Müller, J. Ooms, D. Robinson, D. P. Seidel, V. Spinu, K. Takahashi, D. Vaughan, C. Wilke, K. Woo, H. Yutani, Welcome to the Tidyverse. *J. Open Source Softw.* **4**, 1686 (2019).

60. B. Ripley, *tree: Classification and Regression Trees* (2019); https://CRAN.R-project.org/package=tree.

61. S. Garnier, *viridis: Default Color Maps from "Matplotlib"* (2018); https://CRAN.R-project.org/package=viridis.

62. A. Roesch, H. Schmidbauer, *WaveletComp: Computational Wavelet Analysis* (2018); https://CRAN.R-project.org/package=WaveletComp.

63. D. B. Percival, A. T. Walden, *Wavelet Methods for Time Series Analysis* (Cambridge Univ. Press, 2000); http://ebooks.cambridge.org/ref/id/CBO9780511841040.

64. A. Zeileis, G. Grothendieck, zoo: S3 infrastructure for regular and irregular time series. *J. Stat. Softw.* **14**, 1–27 (2005).

65. J. Bai, P. Perron, Estimating and testing linear models with multiple structural changes. *Econometrica* **66**, 47–78 (1998).

66. D. W. K. Andrews, W. Ploberger, Optimal tests when a nuisance parameter is present only under the alternative. *Econometrica* **62**, 1383–1414 (1994).

67. A. Zeileis, C. Kleiber, W. Krämer, K. Hornik, Testing and dating of structural changes in practice. *Comput. Stat. Data Anal.* **44**, 109–123 (2003).

68. G. Schwarz, Estimating the dimension of a model. *Ann. Stat.* **6**, 461–464 (1978).

69. R. E. Kass, A. E. Raftery, Bayes factors. *J. Am. Stat. Assoc.* **90**, 773–795 (1995).

70. L. Breiman, Ed., *Classification and Regression Trees* (Chapman & Hall [u.a.], 1998).

71. B. Ripley, *Pattern Recognition and Neural Networks* (Cambridge Univ. Press, 1996).

72. W. J. R. M. Priyadarshana, G. Sofronov, Multiple break-points detection in array CGH data via the cross-entropy method. *IEEE/ACM Trans. Comput. Biol. Bioinfirm.* **12**, 487–498 (2015).

73. M. Lavielle, Detection of multiple changes in a sequence of dependent variables. *Stoch. Process. Appl.* **83**, 79–102 (1999).

74. K. Bertin, X. Collilieux, E. Lebarbier, C. Meza, Semi-parametric segmentation of multiple series using a DP-Lasso strategy. *J. Stat. Comput. Simul.* **87**, 1255–1268 (2017).

75. M. Lavielle, Using penalized contrasts for the change-point problem. *Signal Process.* **85**, 1501–1510 (2005).

76. Z. R. Struzik, Wavelet methods in (financial) time-series processing. *Phys. A Stat. Mech. Appl.* **296**, 307–319 (2001).

77. S. Mallat, W. L. Hwang, Singularity detection and processing with wavelets. *IEEE Trans. Inf. Theory* **38**, 617–643 (1992).